INFLUENCE OF THE HALL EFFECT ON THE CHARACTERISTICS OF A MHD GENERATOR WITH TWO PAIRS OF ELECTRODES

E. K. Kholshchevnikova

Zhurnal Prikladnoi Mekhaniki i Tekhnicheskoi Fiziki, Vol. 7, No. 4, pp. 74–84, 1966

The characteristics of segmented-electrode MHD generators with Hall currents are at present the object of considerable interest. Various types of electrode connections are being examined: ordinary segmented-electrode generators, Hall generators, mixed-type generators, and Montardy generators. Research is being pushed in several directions. In some cases infinitely fine segmentation is assumed [1–4].

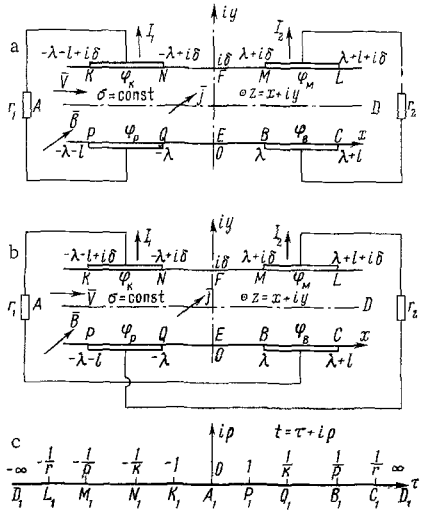

Fig. 1

In these studies it is considered that the current density j in the duct is everywhere uniform; the net characteristics or the most favorable electrode connection angle are determined. In another group of studies periodic problems are solved, it being assumed that the processes taking place in a single elementary cell are repeated in the other cells; fringe effects are not taken into account. In this case it is usually assumed that the lengths of the electrodes and insulators are finite, but small as compared with the duct height [5–7]. Finally, in a last group of studies nonperiodic problems are considered. In [3] Vatazhin solves the problem of the current distribution in a duct with a single pair of electrodes between infinitely long insulators. In [8] a general expression is found for the current density function in the case of an arbitrary number of electrode pairs and for any scheme of electrode connection at finite electrode and insulator dimensions. However, numerical calculations are made only for the periodic problem, whose solution is also obtained in [8]; the effect of segment pitch on the characteristics of a Montardy generator is studied.

The present author has investigated the influence of the Hall effect on the characteristics of a MHD generator having two pairs of electrodes with symmetrical and crossed electrode connections. Although it is obvious that in practice only multisegment ducts will be employed, the examination of a generator with two pairs of electrodes makes possible the qualitative analysis of the various effects observed in segmented-electrode ducts in which the electrodes are connected in different ways. Numerical calculations, based on formulas obtained by solving the corresponding problems, have been made on a M-20 computer. Integrated characteristics of the various generator systems have been obtained as a function of electrode and insulator length, external loads, and Hall parameter ω.

§1. We shall find the solution of the problem of the current distribution in the plane duct of a MHD generator with two pairs of electrodes for the following two cases of electrode connection: a) each pair of symmetrically arranged electrodes is connected across its own external load (Fig. 1a); b) the upper electrode of each pair is connected across the external load with the lower electrode of the adjacent pair (Fig. 1b). For convenience, we shall call the problem of the current distribution in a duct with electrical connection a) problem A, and the problem of the current distribution in a duct with electrical connection b) problem B. In both cases the electrodes of one pair KN and PQ are separated from the electrodes of the other pair ML and BC by insulators NM and QB. At the inlet and outlet of the duct the electrodes are bounded by infinitely long insulators. In the domain of the complex variable $x = x + iy$ the coordinates of the initial and end points of the electrodes are equal to

$$K(-\lambda - l + i\delta),\quad N(-\lambda + i\delta),$$
$$M(\lambda + i\delta),\quad L(\lambda + l + i\delta)$$
$$C(\lambda + l),\quad B(\lambda),\quad Q(-\lambda),\quad P(-\lambda - l).$$

Here l is the length of the electrode, 2λ the length of the insulator, and δ the height of the duct. We denote the currents flowing through the loads r_1 and r_2 by I_1 and I_2.

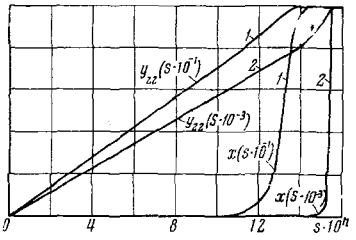

Fig. 2

We solve problems A and B under the following assumptions: the cross-sectional area of the duct, the scalar conductivity of the working medium σ, the magnetic field $B = (0, 0, -B)$ perpendicular to the direction of motion, and the Hall parameter $\omega\tau$ are constant; $\omega_i\tau_i \ll \omega_e\tau_e$, i.e., the ion slip effect can be disregarded; the magnetic Reynolds number is small $R_m \ll 1$, and the induced magnetic field can be neglected; the flow is plane and steady; the velocity of the medium is a known (for example, from the solution in the first approximation of the equations of gas dynamics) function of the coordinates $V = V(x, y)$; the dimension of

the duct in the direction of the magnetic field is taken equal to unity.

With these assumptions the current density j and the potential φ are determined from the system of equations:

generalized Ohm's law

$$\mathbf{j} = \sigma\left(-\nabla\varphi + \frac{1}{c}\mathbf{V}\times\mathbf{B}\right) - \frac{\omega\tau}{B}\mathbf{j}\times\mathbf{B}, \qquad (1.1)$$

current continuity equation

$$\operatorname{div}\mathbf{j} = 0. \qquad (1.2)$$

In [9] it was shown that if the magnetic field is uniform ($B = B_0 > 0$) and the velocity components can be written in the form

$$V_x = \partial\psi/\partial y, \quad V_y = -\partial\psi/\partial x, \qquad (1.3)$$

then it is possible to introduce the analytic function

$$W(z) = j_y(z) + ij_x(z). \qquad (1.4)$$

Representation (1.3) is always possible for an incompressible fluid with ρ = const (then ψ is the stream function) and for rectilinear flow at arbitrary velocity $\mathbf{V} = \mathbf{V}(y)$ in a duct of constant cross section. In this case

$$\psi = \int_0^y V\,dy.$$

Let representation (1.3) be possible in our case. We conformally map the strip z onto the half-plane t with the aid of the transformation

$$t = \tau + i\rho = e^{\pi(\lambda+l+z)/\delta}. \qquad (1.5)$$

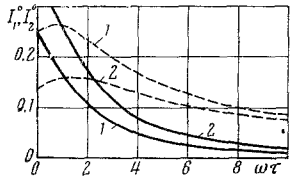

Fig. 3

In this case the function W(z) goes over into the function F(t), and the duct boundary in the z domain goes over into the real axis in the t plane. Transformation (1.5) is illustrated in Fig. 1c. For the parameters k, p, and r, in terms of which the coordinates of the end points of the electrodes in the t plane are determined, we obtain from (1.5) the relations

$$k = e^{-\pi l/\delta}, \quad q = e^{-2\pi\lambda/\delta}, \quad p = kq, \quad r = kp = k^2q. \qquad (1.6)$$

The boundary conditions corresponding to the electrode connections considered have the form

$$\frac{\partial\varphi}{\partial x} = 0, \quad j_x = \omega\tau j_y \quad (KN, ML, BC, PQ), \qquad (1.7)$$

$$j_y = 0 \quad (-\infty K, NM, L\infty, \infty C, BQ, -P\infty), \qquad (1.7)$$

$$j_x = j_y = 0 \quad (F(t) = 0) \quad (x = \pm\infty), \qquad \text{(cont'd)}$$

$$I_1 r_1 = \varphi_K - \varphi_P, \quad I_2 r_2 = \varphi_M - \varphi_B, \quad I_1 = \int_{-1}^{-1/k} j_y(\tau, 0)\frac{\partial x}{\partial\tau}\,d\tau = \int_{1}^{1/k} j_y(\tau, 0)\frac{\partial x}{\partial\tau}\,d\tau \quad (A), \qquad (1.8)$$

$$I_1 r_1 = \varphi_K - \varphi_B, \quad I_2 r_2 = \varphi_M - \varphi_P, \quad I_1 = \int_{-1}^{-1/k} j_y(\tau, 0)\frac{\partial x}{\partial\tau}\,d\tau = \int_{1/p}^{1/r} j_y(\tau, 0)\frac{\partial x}{\partial\tau}\,d\tau. \quad (B). \qquad (1.9)$$

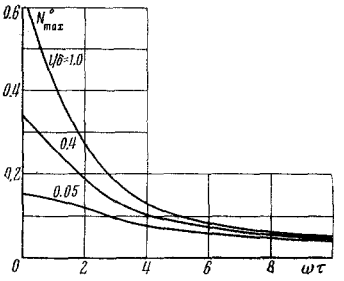

Fig. 4

Here the potentials on electrodes KN, ML, BC, PQ, which are assumed to be ideal conductors, have been denoted respectively by φ_K, φ_M, φ_B, and φ_P. For the t region boundary conditions (1.7) can be written in the form

$$a(\tau)\,j_y(\tau) + b(\tau)\,j_x(\tau) = c(\tau), \qquad (1.10)$$

where $a(\tau)$, $b(\tau)$ and $c(\tau)$ are given functions of τ.

The problem of finding a function (1.4) analytic in the upper half-plane and satisfying boundary condition (1.10) is a Riemann-Hilbert boundary value problem. The general form of the solution of this problem for an arbitrary number of electrode pairs and an arbitrary electrode connection scheme was obtained in [8]. For our specific case (duct with two pairs of electrodes) the function F(t), obtained from the general solution, is equal to

$$F(t) = j_y(t) + ij_x(t) = i\,(t-L_1)^{-\nu/\pi-1}(t-M_1)^{\nu/\pi}\times \times(t-N_1)^{-\nu/\pi-1}(t-K_1)^{\nu/\pi}\times \times(t-P_1)^{-\nu/\pi-1}(t-Q_1)^{\nu/\pi}(t-B_1)^{-\nu/\pi-1}\times \times(t-C_1)^{\nu/\pi}t(R_1+R_2t+R_3t^2) \qquad \left(\nu = -\operatorname{arc\,tg}\left(\frac{1}{\omega\tau}\right), \quad -\frac{1}{2} \leqslant \frac{\nu}{\pi} < 0\right). \qquad (1.11)$$

The constants R_1, R_2, and R_3 in (1.11) are determined for problem A from conditions (1.8), and for problem B from conditions (1.9). The ends of the electrodes in the t plane are denoted by the letters L_1, M_1, ..., C_1 (Fig. 1c). In using Eq. (1.11) these letters must be replaced with the coordinates of the corresponding points in the t plane.

After rather laborious transformations it is possible to obtain the following equations for the integrated generator characteristics:

$$I_1^\circ = \frac{r_2^\circ + \beta e^\circ}{\Lambda}, \quad I_2^\circ = \frac{r_1^\circ + \beta g^\circ}{\Lambda}, \quad N^\circ = I_1^{\circ 2} r_1^\circ + I_2^{\circ 2} r_2^\circ,$$

$$Q = \int_0^{\delta} \int_{-\infty}^{+\infty} \frac{j^2}{\sigma}\, dx\, dy = E(I_1 + I_2) - N,$$

$$\eta = \frac{N}{N+Q} = \frac{N^\circ}{I_1^\circ + I_2^\circ}. \qquad (1.12)$$

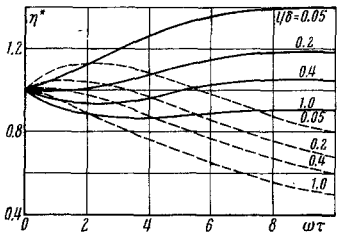

Fig. 5

Here r° is the dimensionless load, I° the dimensionless current, N° the dimensionless power, η the efficiency, E the generator emf, Q the Joule dissipation, Ω the volume flowrate:

$$E = \frac{B}{c}\int_0^{\delta} V_x\, dy = \frac{B}{c}\Omega = \text{const}, \quad r^\circ = \sigma r,$$

$$I^\circ = \frac{I}{\sigma E}, \quad N^\circ = \frac{N}{\sigma E^2},$$

$$\Lambda = r_1^\circ r_2^\circ + \beta b^\circ r_1^\circ + \beta c^\circ r_2^\circ + \beta^2 d^\circ, \qquad \beta = \sqrt{1 + \omega^2\tau^2},$$

$$b^\circ = \frac{b}{a}, \quad c^\circ = \frac{c}{a}, \quad d^\circ = \frac{d}{a}, \quad e^\circ = \frac{e}{a}, \quad g^\circ = \frac{g}{a}.$$

The coefficients a, b, c, d, e and g for problems A and B are different and constitute sets of definite integrals, which are obtained in writing the function F(t) (1.11) on different sections of the duct boundary in the t plane. These definite integrals, and hence the coefficients a, b, c, d, e and g, depend on the parameters k, q, p, r and ν, i.e., on the geometrical dimensions of the duct l/δ and λ/δ and the Hall parameter $\omega\tau$. Altogether, there are 21 such integrals. In order to investigate the effect of the external loads, the relative dimensions of the electrodes and insulators, and the Hall parameter on the generator characteristics, it is necessary to compute the values of these integrals at different values of the parameters l/δ, λ/δ and $\omega\tau$. The evaluation of the integrals is the most complicated part of the problem. This is because it is necessary to evaluate a large number of integrals, whose integrands are represented by quite clumsy expressions, while the capacity of the computer memory is relatively small. Moreover, the integrand functions have singularities at the upper and lower limits of integration, as a result of which the computation process is attended by a number of difficulties, which, however, it has proved possible to overcome. The method of evaluating the integrals is explained in detail in § 2 below.

§2. All the integrals entering into the solution can be reduced to integrals whose lower limit of integration is equal to zero, while the upper limit is equal to unity:

$$Ji = \int_0^1 f_i(x)\, dx \qquad (i = 1, \ldots, 21). \qquad (2.1)$$

The functions $f_i(x)$ go to infinity at the upper and lower limits of integration. By way of example, we write out one of them:

$$f_1(x) = \left\{ x^{-\frac{\nu}{\pi}} (1-x)^{\frac{\nu}{\pi}+1} (1-k)^3 \left[\left(\frac{1-r}{1-k} - px\right) \times \right.\right.$$

$$\times \left(\frac{2k}{1-k} + x\right)\left(\frac{1+p}{1-k} + qx\right)\Big]^{\frac{\nu}{\pi}+1} \times$$

$$\left.\left. \times \left[\left(\frac{1-p}{1-k} - qx\right)\left(\frac{1+k}{1-k} + x\right)\left(\frac{1+r}{1-k} + px\right)\right]^{-\frac{\nu}{\pi}} \right\}^{-1}.$$

We find the integrals (2.1) by integrating the system of ordinary equations

$$\frac{dy_i}{dx} = f_i(x) \quad \left(y_i(x) = \int_0^x f_i(t)\, dt\right) \qquad (2.2)$$

satisfying the boundary conditions $y_i(x = 0) = 0$, up to the value x = 1. In order to get rid of the singularities in the right sides of the differential equations, we make the change of variables

$$ds = \left(\sum_i f_i^2(x) + 1\right)^{1/2} dx. \qquad (2.3)$$

Substituting for $f_i(x)$ in (2.3), after transformations we obtain

$$\frac{dx}{ds} = \frac{1}{L}\left[x^{\frac{\nu}{\pi}+1}(1-x)^{\frac{\nu}{\pi}+1}\right]. \qquad (2.4)$$

Here L is a complex function of x and the parameters k, q, p, r and ν, without singularities on the interval [0, 1]. Substituting (2.4) in (2.2), we have

$$\frac{dy_i}{ds} = \frac{1}{L}\left[f_i(x)\, x^{\frac{\nu}{\pi}+1}(1-x)^{\frac{\nu}{\pi}+1}\right] \qquad (i = 1, \ldots, 21). \quad (2.5)$$

Let $s(x = 0) = 0$. In the integration of system of equations (2.4), (2.5), equivalent to (2.2), the independent variable s takes values ranging from $s = 0$ to $s = s^*$, the value at which x becomes equal to 1. The boundary conditions take the form

$$y_i(s = 0) = 0, \qquad y_i(s = s^*) = J_i. \qquad (2.6)$$

If we integrate system (2.4), (2.5) by the Runge-Kutta method, it is impossible to get away from the initial point $x_0 = 0$ by giving an increment to the argument s, since $(dx/ds)_{x=x_0} = 0$. Therefore we reduce Eq. (2.4) to the form

$$\frac{dy_{22}}{ds} = \frac{1}{L}\left[-\frac{\nu}{\pi}(1-x)^{\frac{\nu}{\pi}+1}\right] \qquad (y_{22} = x^{-\nu/\pi}). \quad (2.7)$$

Thus, it is necessary to integrate system of differential equations (2.5), (2.7) satisfying boundary conditions (2.6). The right sides of system (2.5), (2.7) are free of singularities over the entire interval of integration; therefore the system can be numerically integrated on an electronic computer using known standard programs.

We note that after replacement of the variable of integration x by the variable s the right sides of certain equations of system (2.5), (2.7) were found to depend on cofactors of the type $(1 - x)^\alpha$ $(0 \le \alpha < 1)$, while the right sides of the other equations were found to be independent of these cofactors. Consequently, toward the end of the interval of integration, as $x \to 1$, the derivatives of certain functions with respect to s tend to zero (we will call these functions of the first group); the derivatives of the other functions (we shall call these functions functions of the second group) tend to finite nonzero values as $x \to 1$. From the results of preliminary calculations of the system (2.5), (2.7) on a M-20 computer by the Runge-Kutta method we constructed graphs of x(s) and $y_{22}(s)$ for two cases (Fig. 2). Curves 1 correspond to values of the parameters $l/\delta = 0.4$, $\lambda/\delta = 0.01$, $\omega\tau = 5$ ($x = y_{22}^{1.5 \cdot 9}$); curves 2 correspond to values of the parameters $l/\delta = \lambda/\delta = 1$, $\omega\tau = 10$ ($x = y_{22}^{31.5}$) $\varepsilon_1 = 10^{-8}$. It is clear from (2.7) and Fig. 2 that x(s) and $y_{22}(s)$ are functions of the first group. Since the values s^* at which it is

necessary to terminate the calculation are different for different values of the parameters l/δ, λ/δ and $\omega\tau$ and are not known in advance, system (2.5), (2.7) was calculated with automatic selection of the interval and standard estimation of the relative error. After each step the computed value of x was compared with unity; the calculation was stopped when the condition $|1 - x| < |\varepsilon_1|$ was satisfied, where ε_1 is the given error. It is clear from the above that a small deviation of the final value of x from unity may lead to a considerable error in determining the final value of s. We shall denote this error by Δs^*. The errors in the functions y_i associated with inaccurate determination of s^* can be determined from the equation

$$\Delta y_i = \left(\frac{dy_i}{ds}\right)_{s^*} \Delta s^* .$$

Hence it is clear that the errors of the functions of the first group are close to zero, while the errors of the functions of the second group are finite and proportional to Δs^*. Preliminary calculations showed that for the minimum permissible value of ε_1 for the M-20 computer the errors of functions of the second group are intolerably large.

Moreover, as a result of preliminary calculations it was found that automatic step selection in calculating the system (2.5), (2.7) with the maximum possible accuracy for the M-20 does not always ensure a given accuracy (to the fifth place) of determination of the functions y_i. This may be explained as follows: it is clear from Fig. 2 that the functions y_{22} varies quite uniformly with respect to s; on the other hand, the function x(s) is highly nonuniform: on a large part of the interval of integration x varies extremely little, but then increases rapidly to unity. In this case the relation x(s) is the more nonuniform and differs the more sharply from the nature of the relation $y_{22}(s)$, the greater $\omega\tau$ (see (2.7)).

In view of the fact that for the selection of a new step the calculation error is estimated only for the functions y_i ($i = 1, \ldots, 22$) entering into system (2.5), (2.7), automatic step selection is not accompanied by refinement of the step in the region of rapid variation of x. This means that in a number of cases the relation x(s), and hence the functions y_i, are inaccurately determined. Therefore it is necessary to introduce artificial refinement of the integration step to correspond with the nature of the x(s) curve.

For a more accurate determination of the functions y_i it is possible to carry out the calculation in the following order. From the x(s) curve constructed as a result of a preliminary calculation of the least favorable case, corresponding to maximum values[1] of the parameters l/δ, λ/δ, and $\omega\tau$, we find a series of reference points, in passing through which the step must be refined. It should be kept in mind that for different values of l/δ, λ/δ, and $\omega\tau$ the value of s, near which x begins to increase sharply, is different and is displaced in the direction of large s with increase in $\omega\tau$; at small $\omega\tau$ there may be no interval of rapid variation of x at all.

Accordingly, we selected three reference values of x, with which we compared the values of x computed in each integration step. As before, the calculation was conducted in accordance with the Runge-Kutta method. The step h was determined as follows: h is selected automatically at $x < 0.0001$

$$\begin{array}{ll} h = 0.02 \quad s_+ & (0.0001 < x < 0.1), \\ h = 0.001 \quad s_+ & (0.1 < x < 0.7), \\ h = 0.0002 \quad s_+ & (0.7 < x < 1.0). \end{array} \qquad (2.8)$$

Here s_+ is the value of the argument at which the value of x first exceeded 0.0001. The calculation was stopped when the condition $|1 - x| < |\varepsilon_1|$ was satisfied. The functions of the first group $y_i(s^*)$ were taken equal to the values of the unknown integrals J_i. In order to eliminate the error in calculating the functions of the second group at the end of the integration interval the following method was employed.

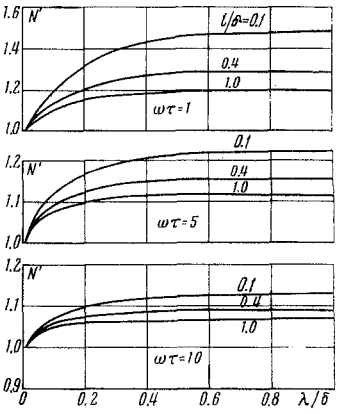

Fig. 6

The values of x computed in each step were compared with a certain value x^* close to unity. Preliminary calculations showed that the given calculation accuracy is achieved when x^* lies in the interval $0.999 \leq x^* \leq 0.9999$. When the condition $|x^* - x| < |\varepsilon_2|$, where ε_2 is the given error, was satisfied, the values of the functions $y_i(x)$ were stored in a certain block of cells. Upon completion of the calculation of system (2.5), (2.7) Simpson's method was used to find the value of one of the integrals of the second group, for example, J_1. From this value the values of the other integrals of the second group were corrected. The integral J_1 can be represented as the sum of two integrals

$$J_1 = \int_0^1 f_1(x)\,dx = \int_0^{x^*} f_1(x)\,dx + \int_{x^*}^1 f_1(x)\,dx = y_1(x^*) + Y_1 .$$

The integral Y_1 was computed from a standard program by Simpson's method.

We divide the differential equations of system (2.5), (2.7) by the first equation

$$\frac{dy_i}{dy_1} = \mu_i(x) \qquad (i = 1, \ldots, 21) .$$

Here $\mu_i(x)$ is the ratio of the right side of the i-th equation to the right side of the first equation. Preliminary calculations showed that the functions $\mu_i(x)$ vary little at values of x close to unity. Therefore they can be replaced by the mean value

$$\langle \mu_i \rangle = 0.5\ [\mu_i(x^*) + \mu_i(1)] .$$

Then for the increments of the functions y_i on the interval $[x^*, 1]$ we obtain

$$\Delta y_i = \langle \mu_i \rangle\ \Delta y_1 = \langle \mu_i \rangle\ Y_1 ,$$

and the values of the unknown integrals of the second group will be equal to

$$J_i = y_i(x^*) + \Delta y_i .$$

Preliminary calculations showed that the calculation method described makes it possible to obtain values of the integrals J_1 with given accuracy (to the fifth place). However, refinement of the step in the sequence (2.8) leads to a considerable increase in the time required to compute the variants (one variant corresponds to the assigment of values of the three parameters l/δ, λ/δ and $\omega\tau$), in which the function x(s) is sufficiently uniform.

Thus, in computing with automatic step selection one such variant is computed in 1–3 min, while in computing with progressive refinement of the step the time required is 15–30 min. Therefore, it is

[1] An estimate of the values of the integrals at different values of l/δ, and λ/δ showed that at $l/\delta > 1$ or $\lambda/\delta > 1$ overflow is possible; therefore $(l/\delta)_{max} = (\lambda/\delta)_{max} = 1$. When $\omega\tau > 10$, the ion slip effect beomces appreciable; therefore $\omega\tau_{max} = 10$.

desirable to perform the calculation of all variants by the method described with automatic step selection at two different values of s^*, for example, $x^* = 0.5$ and $x^* = 0.999$. In this case at $x^* = 0.5$ the integrals of the second group will be incorrectly evaluated, while at any x^* the integrals of the first group are evaluated in essentially the same way; the only difference is that for storing values of $y_i(x^*)$ at different x^* the step will be refined close to different values of s corresponding to the given x^*.

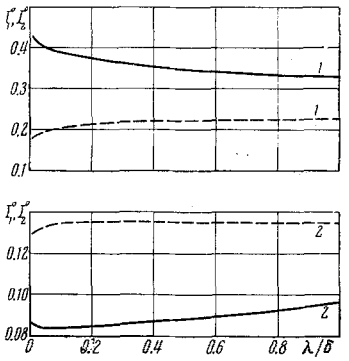

Fig. 7

If automatic step selection ensures the given accuracy, then the first four places of the integrals of the first group, evaluated at two different values of x^*, will coincide. In this case the results of the computation at $x^* = 0.999$ will be correct. If the first four places of the integrals of the first group do not coincide, it will be necessary to recalculate these variants using a program with step refinement in the sequence (2.8).

In this way we calculated the integrated characteristics of MHD generators corresponding to schemes A and B for the following values of the parameters $r_1^\circ = 0, 1, 2, 5, 10, 20$; $r_2^\circ = 0.1, 2, 5, 10, 20$; $\omega\tau = 0, 1, 3, 5, 7, 10$; $l/\delta = 0.05, 0.1, 0.2, 0.4, 0.7, 1$; $\lambda/\delta = 0.01, 0.03, 0.05, 0.1, 0.3, 0.7, 1$. The accuracy of determination of the characteristics lies in the range 1–5%.

§3. We will now analyze the results of the calculation. First, we will consider the influence of the Hall effect on the characteristics of generators A and B in the case of equal external loads $r_1^\circ = r_2^\circ = r^\circ$. Calculations for equal external loads $r^\circ = 5$ were made for problems A and B at different values of the parameters l/δ, λ/δ and $\omega\tau$. The currents I_1° and I_2°, and hence the potential differences between the electrodes connected by loads r_1° and r_2°, for problem A were found to be equal in all cases when $\omega\tau$ was varied from 0 to 10. The corresponding currents and potential differences for problem B were found to be essentially unequal, the values of I_2° and $\Delta\varphi_2^\circ = I_2^\circ r_2^\circ$ ($\varphi^\circ = \varphi/E$ is the dimensionless potential) being always greater than I_1° and $\Delta\varphi_1^\circ = I_1^\circ r_1^\circ$.

In order to elucidate the results obtained, we calculated the values of the electric potentials on the electrodes for several cases, where the values of the constants R_1, R_2, and R_3 computed on the M-20 were known. In this case we assumed that the potential of one of the electrodes was equal to zero ($\varphi_P^\circ = 0$). In MHD generators the direction of the Hall current coincides with the direction of motion of the working medium, i.e., with the direction of the vector V. In the case in question the Hall current flows from left to right. The calculations of the electrode potentials showed that at $\omega\tau \neq 0$ and any values of the parameters l/δ and λ/δ the potentials on the electrodes of the right-hand pair are greater than the potentials on the electrodes of the left-hand pair, i.e., the Hall effect in MHD generators with segmented electrodes leads to an increase in the electric potential along the duct in the direction of motion of the working medium. The longitudinal growth of potential takes place in such a way that the potential differences between opposite electrodes remain constant. As $\omega\tau$ increases, the growth of potential along the length of the duct increases.

Thus, for example, when $l/\delta = \lambda/\delta = 0.1$ for problem A we have $\varphi_B^\circ - \varphi_P^\circ = 0.111$ at $\omega\tau = 1$ and $\varphi_B^\circ - \varphi_P^\circ = 0.585$ at $\omega\tau = 10$; for problem B we have $\varphi_B^\circ - \varphi_P^\circ = 0.0775$ at $\omega\tau = 1$ and $\varphi_B^\circ - \varphi_P^\circ = 0.138$ at $\omega\tau = 10$. We note that in problem A the longitudinal growth of potential is much more intense than in problem B.

The phenomena described can be explained as follows. In MHD generators at $\omega\tau \neq 0$ there appears a Hall emf E^* which causes the positive charges to move in the direction of the vector V. Consequently, there is an increase in the electric potential along the length of the duct in the case of segmented electrodes. When the electrodes are connected in accordance with scheme A, positive particles, migrating from the region of the left-hand pair of electrodes into the region of the right-hand pair under the influence of the Hall emf E^*, cannot return to the left-hand pair. Therefore, in this scheme the potential of the right-hand pair increases until the electric forces due to the longitudinal potential difference balance the action of the Hall forces. Thus, in the steady-state regime the longitudinal potential difference is equal to E^*, and there are no currents flowing from one pair of electrodes to the other. In this case $I_1^\circ = I_2^\circ$, since the potentials of the upper and lower electrodes of the right-hand pair increase by the same amount.

In scheme B the reason for the increase in the potential difference $\Delta\varphi_2^\circ$ and hence in the current I_2°, and the decrease in the potential difference $\Delta\varphi_1^\circ$ and current I_1°, is the increase in the potential of the upper electrode of the pair connected by the load r_2° and the increase in the potential of the lower electrode of the pair connected by the load r_1°. Since in scheme B, $I_2^\circ > I_1^\circ$, I_2° can be written in the form of a sum:

$$I_2^\circ = I_1^\circ + I_3^\circ, \qquad (3.1)$$

where I_3° is the current that flows along the diagonal from electrode PQ to electrode ML. We shall make the conventional assumption that a current source, whose emf is equal to the Hall emf E^*, is located between the two pairs of electrodes. It is known that the maximum potential difference is produced at the terminals of the current source when no current flows. Therefore in scheme A, where $I_3^\circ = 0$, the potential difference in the longitudinal direction will be much greater than in scheme B.

We will consider the influence of the external loads and the parameters l/δ, λ/δ and $\omega\tau$ on the integrated characteristics of MHD generators corresponding to schemes A and B. Calculations showed that, as when $\omega\tau = 0$, in the presence of a Hall effect the power has a maximum with respect to both external loads, i.e., there are optimal loads $r_{1\,opt}^\circ$ and $r_{2\,opt}^\circ$, at which $N^\circ = N_{max}^\circ$. The variation of the efficiency η as a function of r_1° and r_2° is also analogous to the case $\omega\tau = 0$, which was examined in detail in [10]. With increase in both loads η increases and tends to unity as $r_1^\circ \to \infty$ and $r_2^\circ \to \infty$, since in this case the currents and hence the Joule losses tend to zero.

In scheme A the optimal loads with respect to power are equal $r^\circ_{1opt} = r^\circ_{2opt} = r^\circ_{opt}$ and increase with increase in $\omega\tau$ ($r^\circ_{opt} \approx 2$ at $\omega\tau = 0$ and $r^\circ_{opt} \approx 10$ at $\omega\tau = 10$). Since in this scheme $I^\circ_1 = I^\circ_2$ at $r^\circ_1 = r^\circ_2$, the current flowing through each load can be written in the form $I = E/(r + r_i)$, where E is the generator emf, and r_i the internal resistance. It is known from electrical engineering that in such a simple circuit the maximum power is released in the external load when $r = r_i$. With increase in $\omega\tau$ the internal resistance increases due to the increase in the length of the flow lines; therefore the value of the optimal external load also increases.

In scheme B the optimal loads are essentially unequal: $r^\circ_{1opt} < r^\circ_{2opt}$. With increase in $\omega\tau$ r°_{1opt} varies only very slightly: $r^\circ_{1opt} \approx 2-0$ with variation of $\omega\tau$ from 0 to 10, while r°_{2opt} increases from 2 at $\omega\tau = 0$ to 20 at $\omega\tau = 10$; we note that in the great majority of cases $r^\circ_{1opt} \neq 0$. In order to elucidate these results, we will consider the effect of the parameter $\omega\tau$ on the currents I°_1 and I°_2 (Fig. 3). In the graph the continuous lines correspond to the current I°_1, the broken lines to the current I°_2; the numeral 1 denotes curves relating to the case $r^\circ_1 = r^\circ_2 = 2$, numeral 2 denotes curves relating to the case $r^\circ_1 = 1$, $r^\circ_2 = 5$; $l/\delta = 0.2$, $\lambda/\delta = 0.1$. It is clear from the graph that when $r^\circ_1 \leq r^\circ_2$ the current I°_1 always decreases, while the current I°_2 first increases, and then decreases with increase in $\omega\tau$. At large $\omega\tau$ the current I°_2 is always greater than I°_1. The calculations showed that when $r^\circ_1 > r^\circ_2$ both currents I°_1 and I°_2 decrease with increase in $\omega\tau$, but the current I°_2 is always the greater. This variation of the currents as a function of $\omega\tau$ is associated with the following effects: 1) when $r^\circ_1 \neq r^\circ_2$ there exist electric forces that cause current to flow in the direction of the smaller resistance; 2) with increase in $\omega\tau$ the internal r_i increases, as a result of which the currents I°_1 and I°_2 decrease; 3) with increase in $\omega\tau$ the Hall emf E* increases, which increases the current I°_2 and decreases the current I°_1.

Since N° depends on the products of the squares of the currents and the loads, and $I^\circ_2 > I^\circ_1$ at large $\omega\tau$, it is clear that N°_{max} will be attained when the larger current is multiplied by the larger load.

In Fig. 4 the powers N°_{max} of generators A and B are shown as a function of $\omega\tau$ at different values of l/δ and $\lambda/\delta = 0.1$ for loads r°_{1opt} and r°_{2opt}, optimal for the given λ/δ and each value of l/δ and $\omega\tau$. Clearly, N°_{max} decreases sharply with increase in $\omega\tau$. Thus, for example, when $l/\delta = 1$ an increase in $\omega\tau$ from 0 to 10 leads to a decrease in N°_{max} by 92%. It is clear that this decrease in power is associated with an increase in r_i as $\omega\tau$ increases. We note that at large $\omega\tau$ the curves corresponding to different l/δ approach each other, i.e., the influence of the parameter l/δ decreases with increase in $\omega\tau$. Moreover, the parameter $\omega\tau$ has less effect on the characteristics of generators with small l/δ; the power of generators with small l/δ decreases less strongly with increase in $\omega\tau$ than the power of generators with large l/δ.

The efficiency of generators of type A and B with $r^\circ_1 = r^\circ_2$ or $r^\circ_1 > r^\circ_2$ varies as a function of $\omega\tau$ in the same way as N°_{max}. When $r^\circ_1 < r^\circ_2$ the efficiency η in scheme B may have a maximum with respect to $\omega\tau$. The corresponding curves are presented in Fig. 5. Along the ordinate axis we have plotted the quantity $\eta^* = \eta/\eta_{\omega\tau=0}$. The curves have been constructed for two cases: $r^\circ_1 = 1$, $r^\circ_2 = 20$ (continuous lines), and $r^\circ_1 = 1$, $r^\circ_2 = 5$ (broken lines); $\lambda/\delta = 0.1$. The values of N° and η always increase with increase in l/δ owing to the decrease in internal resistance. However the negative influence of $\omega\tau$ is less strongly expressed in relation to the characteristics of generators with smaller l/δ; therefore the η^* curves for smaller l/δ occupy a higher position in Fig. 5. The variation of the η^* vs. $\omega\tau$ curves can easily be explained if one knows the nature of the variation of the currents I°_1 and I°_2 as a function of $\omega\tau$ for cases of unequal loads r°_1 and r°_2.

We will consider the influence of the parameter λ/δ on the characteristics of generators A and B. At equal loads the characteristics of generator A always improve with increase λ/δ, since at large λ/δ current begins to leak into the zone outside the electrodes, which leads to a decrease in internal resistance. When the loads are unequal, the parameter λ/δ affects the characteristics of generator A in the same way as when $\omega\tau = 0$, as a result of which in this scheme the Hall effect does not produce an increase in the current I°_2 as compared with the current I°_1 (see[10]). Figure 6 shows the power $N' = N^\circ/N^\circ_{\lambda/\delta=0.01}$ as a function of λ/δ for generators A and B at loads optimal for each value of l/δ, λ/δ and $\omega\tau$. Clearly, an increase in the length of the insulating gap leads to a considerable increase in power output in the case of optimal resistances. At equal or unequal loads an increase in the parameter λ/δ in generator B may lead to a different form of variation of the power and efficiency: the N° and η curves may be increasing or decreasing, but may also have maxima at certain values of $\omega\tau$. This is associated with the fact that the parameter λ/δ does not have the same effect on the currents I°_1 and I°_2 at different values of $\omega\tau$. Figure 7 presents curves for the currents I°_1 and I°_2 (the current I°_1 is shown by a continuous line, the current I°_2 by a broken line) as a function of λ/δ at $l/\delta = 1$ and $r^\circ_1 = 1$, $r^\circ_2 = 5$ for two values of $\omega\tau$: the numeral 1 corresponds to the case $\omega\tau = 1$, the numeral 2 to be case $\omega\tau = 5$. The curves shown in Fig. 7 may be explained as follows. At small $\omega\tau$ the effect of the electric forces causing a current to flow in the direction of the smaller resistance is greater than the influence of the Hall emf; therefore the current I°_1 is greater than the current I°_2. With increase in the length of the insulator λ/δ the overflow processes are weakened, as a result of which the current I°_1 decreases, while the current I°_2 increases. When $\omega\tau = 5$ the influence of the Hall emf predominates, which leads to an increase in the current I°_2 and a decrease in the current I°_1—here $I^\circ_2 > I^\circ_1$. With increase in λ/δ from zero to a value ~0.05 there is a decrease in the current flow associated with reverse currents flowing from the electrodes at higher potentials to the electrodes at lower potentials (see current flow diagram in [8]), which causes a decrease in the current I°_1 and an increase in the current I°_2. When λ/δ increases to a value of ~0.5, current begins to leak into the zone out side the electrodes, and both currents increase. With further increase in λ/δ the leakage effect becomes much weaker and makes practically no contribution to the currents. The fact that at large λ/δ the current I°_1 does not approach the horizontal asymptote indicates the appearance of effects associated with the action of λ/δ on the Hall emf.

Let us enumerate these effects: 1) the Hall emf increases with increase in λ/δ in the same way as the ordinary emf of a MHD generator increases with in-

crease in duct height; 2) there is an increase in the resistance to overflow of current from one pair of electrodes to the other, as a result of which the current I_3° may decrease; 3) since the current I_3° flows along a flatter diagonal as λ/δ increases, its projection on the y axis decreases; $E^* \sim j_y$ not only in the space of each pair of electrodes but also in the space outside the electrodes; therefore E^* decreases with increase in λ/δ. Since (see (3.1))

$$I_2^\circ = I_1^\circ + I_3^\circ \approx \text{const},$$

while the current I_1° increases, I_3° decreases, i.e., the net result of the above-mentioned effects is a decrease in the Hall emf as λ/δ increases.

Calculations made at equal loads for scheme A, in which $I_3^\circ = 0$, showed that with increase in λ/δ the longitudinal growth of potential increases; consequently, in scheme A an increase in λ/δ leads to an increase in the Hall emf.

The results of calculations of the characteristics of MHD generators of type A for cases when scheme A operates as two independent pairs of electrodes,* were compared with the results obtained on the basis of the asymptotic formula proposed in [3] for large $\omega\tau$. The results of calculations on the M-20 coincided correct to 1% with the calculations based on the asymptotic formula at $\omega\tau = 10$; at $\omega\tau = 5$ the asymptotic formula gives an error of ~8%. With further decrease in $\omega\tau$ the error becomes even greater.

In conclusion, the author thanks A. B. Vatazhin and A. N. Kraiko for their helpful advice.

REFERENCES

1. A. de Montardy, "MHD generator with series connected electrodes," Symposium on Magnetoplasmadynamic Electrical Power Generation, Newcastle, Great Britain, September, 1962.

2. E. N. Zelichenko, T. E. Milleryan, and N. I. Pol'skii, "Optimal regimes for magnetogasdynamic channel flows with Hall effect," Magnitnaya gidrodinamika [Magnetohydrodynamics], no. 1, 67–72, 1965.

3. A. B. Vatazhin, "Some two-dimensional problems of the current distribution in a conducting medium moving through a duct in a magnetic field," PMTF, no. 2, 39–54, 1963.

4. James T. Yen, "Magnetoplasmadynamic channel flow and energy conversion with Hall currents," Phys. Fluids, no. 5, 7, 723–729, 1964.

5. H. Hurwitz, Jr., R. W. Kilb, and G. W. Sutton, "Influence of tensor conductivity on current distribution in a MHD generator," J. Appl. Phys., vol. 32, no. 2, p. 205–216, 1960.

6. E. A. Witalis, "Analysis of linear MHD power generators," Plasma Physics, Accelerators, Thermonuclear Research, J. of Nucl. Energy, pt. C, vol. 7, no. 5, p. 455–473, 1965.

7. E. A. Witalis, "Performance of a segmented electrode MHD generator for various electrode-insulator length ratios," Plasma Physics, Accelerators, Thermonuclear Research, K. Nucl. Energy, pt. C, vol. 7, no. 3, p. 235–244, 1965.

8. I. M. Tolmach and N. N. Yasnitskaya, "Hall effect in a channel with segmented electrodes," Izv. AN SSSR, Energetika i transport, no. 5, 91–104, 1965.

9. A. B. Vatazhin and S. A. Regirer, "Electric fields in MHD channels," supplement to the book by J. A. Shercliff: Electromagnetic Flow-Measurement [Russian translation], Izd. Mir, 1965.

10. E. K. Kholshchevnikova, "Integrated characteristics of a MHD generator with two pairs of electrodes of finite length," PMTF, no. 4, 16–22, 1964.

*Scheme A works as two independent pairs of electrodes under the following conditions: 1) $\lambda/\delta \approx 0.5$–1, any l/δ, $r_1^\circ = r_2^\circ$ or $r_1^\circ \neq r_2^\circ$; 2) $l/\delta \approx 1$, any λ/δ, $r_1^\circ = r_2^\circ$—at large l/δ fringe effects make only a small contribution to the generator characteristics and may be neglected.

6 April 1966 Moscow